

# Indentation and Axial Tests of Two Large-Diameter Tubular Columns

by

Joseph A. Padula  
Alexis Ostapenko

Sponsored by

Minerals Management Service  
of the U.S. Department of the Interior  
(Contract No. 14-12-0001-30288)  
and  
American Iron and Steel Institute  
(Project No. 338)

DOI/AISI COOPERATIVE RESEARCH PROGRAM

Fritz Engineering Laboratory Report No. 508.5

February 1987

# Table of Contents

<b>Abstract</b>	<b>1</b>
<b>1. Introduction</b>	<b>2</b>
<b>2. Description of Test Specimens</b>	<b>4</b>
2.1 Fabrication of Specimens	4
2.2 Dimensions and Material Properties	4
<b>3. Modification of Original Specimens</b>	<b>6</b>
3.1 General Considerations	6
3.2 Determination of the Length of Modified Specimens	6
3.3 Modification Process	8
<b>4. Geometric Measurements</b>	<b>10</b>
4.1 Circumferential Measurements	10
4.2 Longitudinal Measurements	11
<b>5. Indentation of Specimens</b>	<b>12</b>
5.1 General Considerations	12
5.2 Arrangement for Indentation of Specimens	13
5.3 Procedure for Indentation	14
5.4 Results of Indentation	15
5.4.1 Dent Geometry	15
5.4.2 Energy Dissipation	15
<b>6. Axial Load Tests</b>	<b>16</b>
6.1 Test Set-up and Procedure	16
6.2 Instrumentation	16
6.3 Procedure	17
6.4 Specimen Behavior Under Axial Load	17
6.4.1 Specimen P1	17
6.4.2 Specimen P2	18
<b>7. Summary and Conclusions</b>	<b>20</b>
7.1 Introduction and Scope	20
7.2 Indentation and Energy Dissipation	20
7.3 Axial Load Tests	20
7.4 Conclusions	21
<b>8. Acknowledgments</b>	<b>22</b>
<b>References</b>	<b>23</b>

## List of Figures

<b>Figure 1:</b>	Specimen P2 Before Modification	26
<b>Figure 2:</b>	Device Used for Circumferential Measurements of Specimen P2	26
<b>Figure 3:</b>	Location of Strain Gages	27
<b>Figure 4:</b>	Set-up for Indentation of Specimen P1	28
<b>Figure 5:</b>	Axial Load Test Set-up for Specimen P1	28
<b>Figure 6:</b>	Schematic Representation of Ideal Dent Geometry	29
<b>Figure 7:</b>	Schematic Representation of Test Set-up for Indentation	30
<b>Figure 8:</b>	Load-Displacement Curve for Indentation of Specimen P1	31
<b>Figure 9:</b>	Load-Displacement Curve for Indentation of Specimen P2	32
<b>Figure 10:</b>	Contour Plot of Specimen P1 at 0 kN Axial Load	33
<b>Figure 11:</b>	Contour Plot of Specimen P1 at 2230 kN Axial Load	34
<b>Figure 12:</b>	Contour Plot of Specimen P1 at 4450 kN Axial Load	35
<b>Figure 13:</b>	Contour Plot of Specimen P2 at 0 kN Axial Load	36
<b>Figure 14:</b>	Contour Plot of Specimen P2 at 2230 kN Axial Load	37
<b>Figure 15:</b>	Contour Plot of Specimen P2 at 4450 kN Axial Load	38
<b>Figure 16:</b>	Energy Absorption vs. Dent Depth for Specimens P1 and P2	39
<b>Figure 17:</b>	Load vs. Axial Shortening Curve for Specimen P1	40
<b>Figure 18:</b>	Load vs. Axial Shortening Curve for Specimen P2	41
<b>Figure 19:</b>	Formation of Ring Bulge on Specimen P1	42
<b>Figure 20:</b>	Axial Strains, Specimen P1	43
<b>Figure 21:</b>	Axial Strains, Specimen P2	44

## List of Tables

**Table 1:** Specimen Data

25

## Abstract

To investigate the residual strength of damaged offshore structures, tests were conducted on two large diameter tubular steel columns. The test specimens had diameters of 1.02 and 1.53 m (40 and 60 in.) with wall thickness of 6.73 mm (0.265 in.). The corresponding diameter-to-thickness ratios were 151 and 227. The specimens were fabricated by cold-rolling and welding.

A local dent was introduced into each specimen to simulate a damaged member. During this process, data was collected on the denting behavior and energy dissipation characteristics of the specimens. The depth of indentations was 2.7% and 5.5% of the specimen diameter for the smaller and larger diameter specimens, respectively.

Axial load tests were conducted on the dented specimens under fixed-fixed end conditions. The results of the tests showed minimal effect of the indentation on the axial strength of the damaged columns in comparison with the results of tests previously conducted on undamaged specimens. The fixed-fixed end conditions appear to have been the major influence on the relative insensitivity of the specimens to the effects of the indentations.

## 1. Introduction

Offshore platforms may incur structural damage from a number of causes. In addition to operational and environmental loads which in severe cases can overload and consequently damage the structure, an offshore platform may be subjected to ship collision or accidental impact from a falling object. Of these, ship/platform collisions are considered to be the most consequential and appear to occur fairly frequently<sup>1</sup>.

Depending on the type of structure and the cause, damage to a member of an offshore platform may take one of the following forms:

- Local dents in the tube wall
- Overall bending of the member
- Combination of local dents and overall deformation of the member

The degree of damage may vary from slight to a total collapse of the structure although less than severe damage is more common.<sup>1</sup> However, significant damage to offshore platforms occurs in somewhat more than isolated incidences. It has been reported that dents with a depth of 10% of the diameter or permanent deflection of 0.4% of the length of the member occur almost every two years in the North Sea<sup>2</sup>, and there have been a total of 560 various accidents around the world between 1970 and 1981.<sup>1</sup>

Such damage can significantly affect the structural integrity of an offshore platform resulting in the possibility of an accident having serious environmental consequences as well as jeopardizing the safety of its crew. Therefore, assessment of the effect of possible damage should be of concern to engineers involved in the design of offshore structures.

The residual strength of the affected members should be included in the analysis

to determine the overall structural integrity of a damaged platform. A significant amount of research addressing this problem has been undertaken in the last several years.<sup>2, 1, 3, 4, 5, 6, 7, 8, 9</sup> A review of the state of the art has been presented by Ellinas<sup>1</sup>. Probably, the most significant omission in the reported research has been experimental work on tubular members fabricated by cold-rolling and welding, which is the usual method of fabrication for offshore platforms, and the consideration of members with larger diameter-to-thickness ratios.

The experimental work reported here consisted of tests to investigate the behavior and energy dissipation characteristics of large-diameter tubular members during indentation, and the response of the dented members to axial load. The experimental work was conducted on two large-diameter fabricated tubular members with diameter-to-thickness ratios of 151 and 227. The results will be used to verify and fine-tune analytical procedures to be developed subsequently.

## 2. Description of Test Specimens

### 2.1 Fabrication of Specimens

The specimens tested in this study were obtained by modifying two test specimens of a previous project (Specimens T3 and T4 in References 10 and 11). They were fabricated by cold-rolling steel plate into right circular cylinders in a pyramid three-roller bending machine and welding the longitudinal seam by an automatic submerged-arc process. Steel end rings were welded to each end of the specimens to facilitate uniform distribution of the axial load. Detailed information on the fabrication and material properties is given in the above references.

Axial load tests conducted during the previous project resulted in severe local buckles confined to one end of the specimens as shown in Fig. 1 for Specimen T4. Specimen T3 had similar deformations. The limited extent of the deformations made it possible to modify these specimens into new test specimens by removing the buckled portions and reattaching the end rings. The modification process is further described in Chapter 3. After modification, Specimens T3 and T4 were designated P1 and P2, respectively.

### 2.2 Dimensions and Material Properties

Specimens P1 and P2 had outside diameters of 1.02 m (40.2 in.) and 1.53 m (60 in.), respectively. Both specimens had a wall thickness of 6.73 mm (0.265 in.). After modification, Specimen P1 was 2.44 m (96 in.) in length and Specimen P2 2.13 m (84 in.), exclusive of the thickness of the end rings. The circular steel end rings welded to each end of the specimens were 22 mm thick by 127 mm wide (7/8 in. x 5 in.). All pertinent geometric and material properties including diameter-to-thickness ( $D/t$ ), length-to-radius of gyration ( $L/r$ ) and dent depth-to-diameter ( $d/D$ ) ratios are listed in Table 1.

The specimens were fabricated from ASTM A36 steel plate. In the previous project<sup>10</sup>, the static and dynamic yield stresses of the material were determined from standard ASTM coupons. The material properties of the modified specimens, P1 and P2, were assumed to be the same as those of the original specimens. Thus, the possible effects of cold-rolling and work hardening during the original tests were neglected. The static yield stress of 203.8 MPa ( 29.56 ksi) listed in Table 1 is the yield stress at zero strain rate. The dynamic yield stress of 239 MPa (34.67 ksi) was obtained at a strain rate of 1042  $\mu\text{m}/\text{m}/\text{sec}$  (1/16 in./in./min) which corresponds to the highest strain rate effectively permitted by the ASTM A370-77.<sup>12</sup>

### 3. Modification of Original Specimens

#### 3.1 General Considerations

Modification of the test specimens consisted of removing the buckled portion of each specimen and replacing the end ring. The first step in this process was to determine the length of the buckled portion of each specimen to be removed. Primary consideration was given to maximizing the length while limiting the out-of-roundness in the modified specimens. Out-of-roundness is defined by

$$\text{OUT-OF-ROUNDNESS} = \frac{OD_{max} - OD_{min}}{OD_{ave}} \quad (3.1)$$

During modification, one per cent was used as a guideline for the maximum acceptable out-of-roundness.

In determining the location at which to cut the specimens, elastic recovery of deformations due to a release of internal stress resultants at the cut was taken into account. The application of jacking forces was also used as a means of correcting minor out-of-roundness of the cross section after removal of the buckled portion.

#### 3.2 Determination of the Length of Modified Specimens

A computer program for predicting the geometry of a cross section of the specimen at a transverse cut was developed. It was used to determine the length of the modified specimens (or the length of the buckled portion of the specimens to be removed), considering the amount of out-of-roundness practically acceptable in the modified specimen.

The method was based on a rigid frame analysis of a unit width ring of the tube wall located at a transition between the severely buckled and the less deformed portions of the specimen. The following assumptions were made in the analysis:

- The material is elastic-perfectly plastic.
- The specimen cross section was perfectly circular and stress free before buckling.
- The buckling above the ring caused the ring to deform elastically and plastically.
- Deformations of the ring after separation from the buckled portion above were not affected by the restraining effect of the portion of the specimen below the ring.
- The ring recovered elastically after separation from the buckled portion.

Although the ring was assumed to recover elastically, some portions of the ring had yielded making the recovery to a perfect circle impossible. The resultant internal forces were found as redundants by using a force method of indeterminate analysis.

The residual curvature,  $\phi_r$ , of a ring element, originally deformed into the plastic range and fully released elastically after the ring was cut to the "primary structure", is given by the following expression:

$$\phi_r = \phi - \frac{3\epsilon_y}{t} \left[ 1 - \frac{1}{3} \left( \frac{2\epsilon_y}{\phi t} \right)^2 \right]. \quad (3.2)$$

Where  $\phi$  is the initial curvature,  $\epsilon_y$  is the yield strain of the material, and  $t$  is the thickness of the ring. Thus, with the initial curvature and geometric and material properties given, Eq. (3.2) made it possible to calculate the residual curvature of a cut ring. Flexibility coefficients were computed and used in the program to calculate the three redundant forces required to close the ring. The method of virtual work was then employed in the program to calculate the deformed shape of the ring (the shape of the cross section). The output from the program consisted of a series of radial offset distances from a perfect circle to the deformed ring around the circumference.

The following procedure was used to determine the location for cutting the specimen. Curvature measurements were taken around the circumference of the specimen at a location tentatively judged to have sufficiently small deformations. The

method used to make these measurements is described in Section 4.1. The computer program was then used to predict the deformed shape of the cross section as outlined above. If the out-of-roundness was greater than acceptable (considering that minor corrections could be effected) or less than practically necessary, the procedure was repeated with curvature measurements taken at another cross section until an acceptable location for cutting the specimen was found.

### 3.3 Modification Process

The results of the analysis led to the shortening of Specimens P1 and P2 to a length of 2.44 m (96 in.) and 2.13 m (84 in), respectively. This was accomplished by flame cutting around the circumference of the specimens. The end ring was then cut from the removed segment and welded to the cut end of the specimen.

Since, as predicted by the analysis, the out-of-roundness was somewhat excessive after cutting, it was reduced by applying controlled forces in the radial direction at the cut end of the specimen. For Specimen P1, a device made for exactly such a purpose was available from some previous work. It consisted of a wide steel ring fitted with four bolts equally spaced around the circumference and oriented in the radial direction. When the device was placed inside the specimen, tightening the bolts resulted in an outward radial force against the specimen wall. As corrections were made, temporary struts were tack welded inside the specimen to maintain the shape of the cross section after the jacking ring was removed and until the end ring was welded to the specimen. Specimen P2 required relatively little adjustment and the corrective forces were applied with a wooden strut and a hydraulic jack. Jacking at two locations and the installation of temporary bracing were required before the end ring could be welded to the specimen.

The final step in the modification process was the replacement of the end rings

and removal of temporary struts. The cut end of the specimens and end rings were ground flat prior to welding by a manual shielded metal arc process. The temporary bracing was removed after the end rings were tack welded to the specimen. The attachment was then completed with continuous fillet welds on both sides of the specimen wall.

## 4. Geometric Measurements

### 4.1 Circumferential Measurements

Modification of the specimens and establishment of a reference geometry required determination of the cross-sectional profile and curvature. This was accomplished by taking measurements around the specimen circumference.

Two different devices, one for each specimen, were used in making measurements for determining the profile of a cross section as well as the curvature. Both devices essentially established a three point profile of a circumferential arc segment on the specimen surface. For Specimen P1 the measurements were made by employing a hard-board template cut to a circular arc of the specimen radius plus 13 mm (0.5 in.). The distance between the specimen wall and the template edge was measured with a steel rule at mid length of the template. The device used on Specimen P2, an improved version of the device used for P1, is shown in Fig.2. It is more stable and employs a dial gage for faster and more accurate measurements.

Successive overlapping measurements taken around the circumference provided the data for defining the profile of the cross section. They also provided the data for determining the curvature at points around the circumference by the following finite difference equation:

$$y'' = \frac{y_{-1} - y_0 + y_{+1}}{(\Delta x)^2} \quad (4.1)$$

Subtracting the ideal curvature (the reciprocal of the radius) gave the change of curvature around the circumference to be used in the analysis of residual deformations and forces as described in Section 3.2.

After modification of the specimens, circumferential measurements were taken to

establish a reference circle at the ends of each specimen. As a matter of practicality, the measurements were taken 75 mm (3 in.) from each end. From the cross-sectional profile, a reference circle was established at each end of the specimen by the least squares method. These two circles, having a diameter equal to the specimen diameter, defined a reference cylinder.

#### 4.2 Longitudinal Measurements

Longitudinal grid lines were established on the surface of each specimen parallel to each other and separated by  $20^\circ$  of arc dividing the specimen circumference into 18 equal segments. The end points of the grid lines coincided with the points used to establish the reference circle at the ends of the specimens. This allowed the position of the grid lines to be defined with respect to the reference cylinder. The grid lines were consecutively numbered around the specimen circumference starting with No. 1 at the weld seam.

Measurements of the relative position of the specimen wall along the grid lines were made with a dial gage rig consisting of an aluminum framework fitted with mechanical dial gages as shown in Figure 5. The top end of the dial gage rig had a magnet for temporary attachment to the specimen wall. The bottom of the dial gage rig rested on the end ring and was fitted with a leg so that, when positioned on the specimen wall at a grid line, the ends of the rig coincided with the end points of the grid line. This made possible a complete mapping of the surface of the specimen with respect to the reference cylinder.

## 5. Indentation of Specimens

### 5.1 General Considerations

Although damage to a tubular member due to impact may result in localized dents, overall deflection or a combination of both, the experimental phase of this project dealt only with localized denting. Consequently, measures were taken to limit the overall distortion of the test specimens during indentation.

From a review of literature, in particular Reference 13, the ideal geometry of indentation was determined to be a localized flattening of the cylinder surface as shown in Fig. 6. The width of the flat portion of the dent was 175 mm (7 in.). The length of the dent was largely controlled by the depth and was approximately equal to the chord distance subtended by a circular arc with a middle ordinate equal to the depth of the dent.

The dent was located at mid-length of each specimen. To preclude any effects the weld seam might have had on the behavior of the dented specimen, the longitudinal centerline of the dent was offset by  $120^\circ$  of arc from the longitudinal weld seam and thus coincided with grid line No. 7. (The actual location for Specimen P1 was approximately 38 mm (1.5 in.) closer to the weld seam.)

A survey of literature led to the conclusion that the dent depth calculated for Specimen P1 should be 18 mm (0.7 in.) with a corresponding dent depth-to-diameter ratio ( $d/D$ ) of 2%. Considering the results of the axial load test of P1, the intended relative dent depth ( $d/D$  ratio) for Specimen P2 was increased to 5% with a corresponding dent depth of 76 mm (3.0 in.).

## 5.2 Arrangement for Indentation of Specimens

The purpose of the arrangement for indentation was not only to introduce a dent but also to obtain data on the energy dissipation characteristics of the test specimens. The same set-up was used for both specimens; it consisted of a reaction frame, a load transmission assembly and instrumentation.

The set-up was made in a five-million pound universal testing machine which served as the reaction frame. As shown in Fig. 4, the test specimen was placed horizontally on the floor of the testing machine and supported by steel blocks under the end rings. These blocks, in effect, provided simple support at the ends of the specimen and also gave the necessary clearance to place dial gages underneath the specimen.

The load transmission assembly between the machine head and the specimen consisted of a short section of wide flange beam placed transversely across the specimen, a manually operated hydraulic jack, and a load cell. The 175 mm (7 in.) wide flange of the beam served as the die for forming the dent. This arrangement is shown schematically in Fig. 7. Internal bracing in the form of wood or steel struts and transverse bearing members was installed at the edges of the intended indentation in order to localize the deformation. Small hydraulic jacks were used to provide prestress to the bracing members.

The instrumentation for measuring the distortion of the specimens during indentation consisted of ten mechanical dial gages located as shown in Fig. 7. Two were placed between the beam and the testing machine head, one on either side of the jack and load cell. These gages directly measured the extension of the jack and, thus, the displacement relative to the machine head. Four dial gages were placed between the top surface of the specimen and the testing machine head, and three between the test-

ing machine floor and the bottom of the specimen. One dial gage was used to directly measure the displacement of the machine head relative to the floor. This was done by connecting a dial gage mounted on a pedestal on the floor with a light gage wire to a magnetic clip on the testing machine head.

### 5.3 Procedure for Indentation

The indentation procedure consisted of incremental application of load to the specimen through the jack-loadcell-beam assembly. At each load increment, the load and dial gage readings were recorded.

The approximate depth of dent was indicated by the readings from the dial gages between the machine head and the beam. Loading continued until the dent exceeded the desired depth by an amount estimated to be lost due to elastic recovery during unloading. Specimen P1 required two cycles of loading and unloading since the elastic recovery was underestimated in the first cycle. The observed elastic recovery during the first unloading provided a means to estimate more accurately the final depth of dent. The maximum load applied to P1 was 168 kN (37.8 kips). A plot of the load vs. dent depth is shown in Fig. 8.

The set-up and procedure for the indentation of Specimen P2 were similar to those for Specimen P1. During loading of the specimen, at approximately 160 kN (36 kips), one of the wooden struts used for internal bracing failed suddenly. The load immediately dropped to 116 kN (26 kips). The specimen was then unloaded, and the wooden struts were replaced with steel members. Loading then continued to 276 kN (62 kips). The load vs. dent depth response is shown in Fig. 9.

## 5.4 Results of Indentation

### 5.4.1 Dent Geometry

Locally, the depth of dent for Specimen P1 was 19 mm (0.75 in.), with the depth measured with respect to points just outside of the dented area. Subsequent measurements of the specimen geometry with respect to the ends of the specimen showed that the overall depth of indentation was 28 mm (1.1 in.). This indicated that the deformation was a combination of a local dent and an overall deflection of the specimen wall. For Specimen P2, the depth of dent was 84 mm (3.3 in.) overall and 70 mm (2.8 in.) locally. Thus, the nature of the dent was also predominantly local with only slight overall distortion of the specimen. The dentdepth-to-diameter ratios for Specimens P1 and P2 were 2.7% and 5.5%, respectively.

Contour plots of the specimen surfaces of P1 and P2 are given in Figs. 10 and 13. The plots depict the surface of the unfolded cylinder with the horizontal and vertical axes representing the bottom of the specimen and the weld seam, respectively.

### 5.4.2 Energy Dissipation

The amount of energy dissipated during the indentation process was determined from the area under the curve plotted from the load vs. dent depth data. Figure 16 shows the total energy absorbed vs. the dent depth for each specimen. The total energy absorbed, including both the elastic and plastic deformations, was calculated since this would be of interest in considering the mechanics of a collision. The similarity of the two curves over the range shown should be noted.

## 6. Axial Load Tests

### 6.1 Test Set-up and Procedure

The axial load tests were conducted in a Baldwin 5 million pound universal testing machine. The specimens were centered on the floor of the testing machine with the indentation facing forward for ease of observation as shown in Fig 5.

To insure uniform application of load around the circumference of the specimen, each end was set in grout<sup>\*</sup>. This was accomplished by placing the bottom of the specimen in a bed of grout, applying a layer of grout to the top of the specimen, and lowering the machine head until the grout fully filled the gaps between the specimen ends and the machine surfaces. The grout was then allowed to set before actual loading of the specimen began.

### 6.2 Instrumentation

Instrumentation for the axial load test consisted of mechanical dial gages, electric-resistance strain gages, and the load indicator of the testing machine. Three mechanical dial gages with a resolution of 0.025 mm (0.001 in.) were equally spaced around the circumference to measure the overall axial shortening of the specimen. These gages were placed on the end rings of the specimen with thin wires connecting the gages on the bottom end ring to a magnetic clip on the top end ring. Electric resistance strain gages with a 10 mm (0.40 in.) gage length were placed on the inside and outside surfaces of the specimen in the longitudinal direction at each of the eight locations shown in Fig. 3.

Lateral deflection of the specimen wall was measured by means of a movable dial

---

<sup>\*</sup> Hydro-Stone by United States Gypsum Co.

gage rig described in Section 4.2 and shown in Fig. 5. Nine dial gages were equally spaced over the length of the rig for testing Specimen P1. Seven gages were used for Specimen P2 due to its shorter length. The rig was positioned vertically at the grid lines and readings were taken from the dial gages to determine displacement of the specimen wall relative to the end points of the grid lines. Prior to taking readings on the specimen, reference readings were taken against a flat surface.

### 6.3 Procedure

Following the grouting of the specimen in the testing machine, "zero" reference readings were taken from the dial gages, the strain gages, and the dial gage rig. The compressive axial load was slowly applied in increments of 223 and 445 kN (50 and 100 kips); 223 kN (50 kip) increments were used near the initial and final loads and 445 kN (100 kip) increments in-between. At each load increment, readings were taken of the strain gages and of the longitudinal dial gages. Measurements of the lateral deformation of the specimen wall were made with the dial gage rig at each load increment at selected grid lines and especially in the vicinity of the dent. The procedure was repeated until the ultimate capacity of the specimen was reached.

### 6.4 Specimen Behavior Under Axial Load

#### 6.4.1 Specimen P1

The axial behavior of the specimens can be described by the load vs. axial deformation relationship. For Specimen P1, the load-deformation curve, shown in Fig. 17, was essentially linear up to approximately 85% of the ultimate load with only a slight deviation from linearity near the ultimate load of 4573 kN (1028 kips). There was virtually no reduction in the ultimate axial capacity when compared to the previous test of the specimen.<sup>10</sup> Surface rust was observed flaking off the specimen after the load reached 4450 kN (1000 kips). This indicated local yielding of the specimen wall. The

ultimate load was reached with no other observable effects other than a general amplification of the indentation. Immediately after reaching its peak value, the load began to diminish at an approximate average rate of 45 kN/min (10 kips/min). As the load dropped to 3780 kN (850 kips), a ring bulge was observed at the bottom of the specimen as shown in Fig. 19. The ring bulge seemed to have initiated at a point opposite from the indentation and then propagated in both directions around the circumference. However, no buckle appeared in the area directly below the dent.

The effect of axial load on the indentation for Specimen P1 may be seen in the contour plots of the unfolded specimen surface shown in Figs. 10 to 12. Figure 10 shows the surface geometry under zero load while Figs. 11 and 12 are plots at 222 kN (500 kips) and 445 kN (1000 kips), respectively. Comparison of contour lines at successive load levels indicates an increase in the dent depth of approximately 40%.

A plot of the strain gage readings taken from the gages at mid-height of the specimen is shown in Fig. 20. The points plotted give the averages of longitudinal strain through the wall thickness. As expected, there is a significant reduction in the average strain at the dent. However, the actual gage readings indicate considerable bending in the wall.

Shortly after the formation of the ring bulge was observed and before any further distortion was induced, the specimen was unloaded in four steps. This was done in the hope of later retesting the specimen under different end conditions.

#### 6.4.2 Specimen P2

The load-deformation curve for Specimen P2, shown in Fig. 18, was also linear up to approximately 80% of the ultimate load. There was then a slight deviation from linearity before the ultimate load was reached.

As the load was increased to 4890 kN (1100 kips), surface rust was observed flaking off the specimen near the bottom of the specimen. The pattern was indicative of the yielding due to the formation of a ring bulge in this area. The load was increased to 5340 kN (1200 kips) with only further flaking off of surface rust. The ultimate load of 5425 kN (1220 kips) was reached during the next increment and was marked by an immediate reduction of the load and the formation of a ring bulge at the bottom of the specimen. The maximum load reached represents only a 6% reduction in ultimate axial capacity when compared to the previous test of the specimen.<sup>10</sup> As the load continued to drop, a buckle formed at approximately mid-height near the edge of the indentation on grid line 9. A second ring bulge then formed at the top of the specimen. As the load continued to drop, hexagonal lobular buckles proceeded forming over a 20 minute period. The load finally stabilized at 1060 kN (238 kips) with no further buckling of the specimen. Unfortunately, in the course of these deformations, the stroke of the longitudinal dial gages was exceeded, and the total axial shortening at the stabilized load could not be determined from the gages. The portion of the curve beyond the ultimate load in Fig. 18 was constructed by measuring the final length of the unloaded specimen and adjusting for the axial elastic elongation corresponding to the load of 1060 kN (238 kips).

A plot of data taken from the strain gages at mid-height of the specimen is shown in Fig. 21. It shows that there was virtually no increase in the average longitudinal strain at the dent with increasing load. However, considerable bending at the dent was indicated by the strains recorded.

Contour plots of the unfolded specimen surface at three load increments are shown in Figs. 13 to 15. No significant variation in the surface geometry or dent depth was observed under increasing axial load up to the ultimate load.

## 7. Summary and Conclusions

### 7.1 Introduction and Scope

In addition to operational and environmental loads, which in severe cases can overload and damage the structure, an offshore platform may be subjected to ship collisions or accidental impacts from falling objects. Such damage can significantly affect the structural integrity of an offshore platform. The current research on the residual strength of damaged tubular members was undertaken for this reason.

The experimental phase consisted of the introduction of controlled indentations into and axial load tests on two large-diameter short tubular steel columns. The test specimens were fabricated by cold-rolling steel plate into cylinders and welding the longitudinal seam as is typical in the construction of offshore structures.

### 7.2 Indentation and Energy Dissipation

To simulate damaged members in an offshore structure, a dent was introduced into the specimen wall through the application of a transverse load. In the course of indentation, data was collected for the analysis of the energy dissipation characteristics of the test specimens. The results of the analysis showed that the energy dissipation of the two specimens was essentially the same over the range for which data was collected.

### 7.3 Axial Load Tests

The dented specimens were then subjected to axial load tests under fixed-fixed end conditions. Specimen P1 showed no reduction in ultimate axial capacity when compared to the results of the original test on the undented specimen.<sup>10</sup> The mode of failure for Specimen P1 (the formation of a ring bulge at the bottom of the specimen) was the same as in the previous test. The ultimate load attained for Specimen P2

showed only a 6% reduction compared to the original test. Although a lobular buckle formed near the dent, it was preceded by the formation of a ring bulge at the bottom of the specimen which was also the mode of failure in the original test.

Lateral deformation of the specimen wall at the dent was observed to be different for the two specimens. Specimen P2 had virtually no increase in the dent depth with increase of axial load. Whereas, Specimen P1 showed an increase of 40% in the depth of the dent before the ultimate load was reached. However, the growth of dent depth was not accompanied by any reduction of the ultimate strength.

#### **7.4 Conclusions**

The results of the experimental work performed on the two specimens generally indicate that the dents had very little or no effect on the strength of the specimen under axial load. Specifically, the insignificant reduction of ultimate strength and the formation of ring bulges at considerable distance from the dents indicate the minimal effect of the indentations.

It is suspected that the fixed-fixed column end conditions and the short length of the specimen were a major influence on the modes of failure and the relative insensitivity of the specimens to the presence of dents. It is expected that pinned-pinned column end conditions would have led to more pronounced effect of the dent on the behavior of the specimens. The analytical work to be performed should indicate the validity of this expectation.

## 8. Acknowledgments

The authors are grateful to the Minerals Management Service of the Department of the Interior (Contract No. 14-12-0001-30288) and the American Iron and Steel Institute (AISI Project 338) for the support of this work under the DOI/AISI Cooperative Research Program. In particular, thanks are due to C.E. Smith and A.C. Kuentz, the respective representatives of these organizations. The advice and guidance generously given by the members of the Task Force of this project are sincerely acknowledged. The members of the Task Force are: R.H. Wildt (Chairman) of Bethlehem Steel Corporation, Inc., C. Capanoglu of Earl and Wright, A.C. Kuentz of the American Iron and Steel Institute, C.D. Miller of CBI Industries, Inc., J. de Oliveira of Conoco, Inc., and C.E. Smith and J.B. Gregory, both of the Minerals Management Service of the U.S. Department of the Interior.

## References

1. Ellinas, C.P., and Valsgard, S., "Collision and Damage of Offshore Structures: A State-of-the-Art." *Proceedings of the Fourth International Offshore Mechanics and Arctic Engineering Symposium, Vol. 2*. American Society of Mechanical Engineers, New York, February 1985, pp. 475-495, (Symposium held in Dallas, TX, on February 17-21, 1985)
2. Taby, J., and Moan, T., "Collapse and Residual Strength of Damaged Tubular Members." in *Behaviour of Offshore Structures*, Elsevier Science Publishers B.V., Amsterdam, 1985, pp. 395-408.
3. Ellinas, C.P., "Ultimate Strength of Damaged Tubular Bracing Members," *ASCE Journal of Structural Engineering*, Vol. 110, No. 2, February 1984, pp. 245-259.
4. Richards, D.M., and Andronicou, A., "Residual Strength of Dented Tubulars: Impact Energy Correlation," *Proceedings of the Fourth International Offshore Mechanics and Arctic Engineering Symposium, Vol. 2*, American Society of Mechanical Engineers, New York, February 1985, pp. 518-527, (Symposium held in Dallas, TX, on February 17-21, 1985)
5. Ueda, Y., and Rashed, S.M.H., "Behavior of Damaged Tubular Structural Members," *Proceedings of the Fourth International Offshore Mechanics and Arctic Engineering Symposium, Vol. 2*, American Society of Mechanical Engineers, New York, February 1985, pp. 528-536, (Symposium held in Dallas, TX, on February 17-21, 1985)
6. Foss, G., and Edvardsen, G., "Energy Absorption during Ship Impact on Offshore Steel Structures." *Proceedings of the 14-th OTC*, Offshore Technology Conference, Houston, May 1982, pp. (Vol.1)625-634, (Paper 4217)
7. Smith, C.S., "Strength and Stiffness of Damaged Tubular Beam Columns." *Offshore Structures Engineering III --- Buckling of Shells in Offshore Structures*, Harding, J.E., Dowling, P.J., and Agelidis, N., ed., Gulf Publishing Co. (also, Granada Publishing), Houston, London, Paris, Tokyo, 1982, pp. 1-23. (Proceedings of the conference held in April 1981 at Imperial College, London)
8. Smith, C.S., Somerville, W.L. and Swan, J.W., "Residual Strength and Stiffness of Damaged Steel Bracing Members," *Proceedings of the 13th Offshore Technology Conference*, Offshore Technology Conference, Houston, May 1981, pp. 273-282. (Paper OTC 3981)
9. Taby, J., Moan, T., and Rashed, S.M.H., "Theoretical and Experimental Study of the Behaviour of Damaged Tubular Members in Offshore Structures," *Norwegian Maritime Research*, Vol. 9, No. 2, 1981, pp. 26-33.
10. Ostapenko, A., and Grimm, D.F., "Local Buckling of Cylindrical Tubular Columns Made of A-36 Steel," Fritz Engineering Laboratory Report No. 450.7, Lehigh University, February 1980.
11. Grimm, D.F., and Ostapenko, A., "Local Buckling of Steel Tubular Columns." *Proceedings*, Structural Stability Research Council, Bethlehem, PA, 1982, pp. 25-28.

12. American Society for Testing and Materials, *1985 Annual Book of ASTM Standards*, American Society for Testing and Materials, Philadelphia PA, . Vol. 03.01 Metals-Mechanical Testing; Elevated and Low Temperature Tests, 1985.
13. Smith, C.S., "Assessment of Damage in Offshore Steel Platforms." *Proceedings of International Conference on Marine Safety*, . Glasgow, England, September 1983, pp. 279-307.

**Table 1:** Specimen Data

Spec. No.	$F_{ys}$	Dimensions					Dent Depth		Axial Load	
		OD	t	L	D/t	L/r	d	d/D	Present	Previous
	(MPa)	(m)	(mm)	(m)			(mm)	(%)	(kN)	(kN)
P1	203.8	1.02	6.73	2.44	150.7	6.80	28	2.7	4570	4400
P2	203.8	1.53	6.73	2.13	226.5	3.96	85	5.5	5425	5800
	(ksi)	(in.)	(in.)	(in.)			(in.)	(%)	(kips)	(kips)
P1	29.56	40.2	0.265	96.0	150.7	6.80	1.1	2.7	1028	990
P2	29.56	60.3	0.265	84.0	226.5	3.96	3.3	5.5	1220	1300

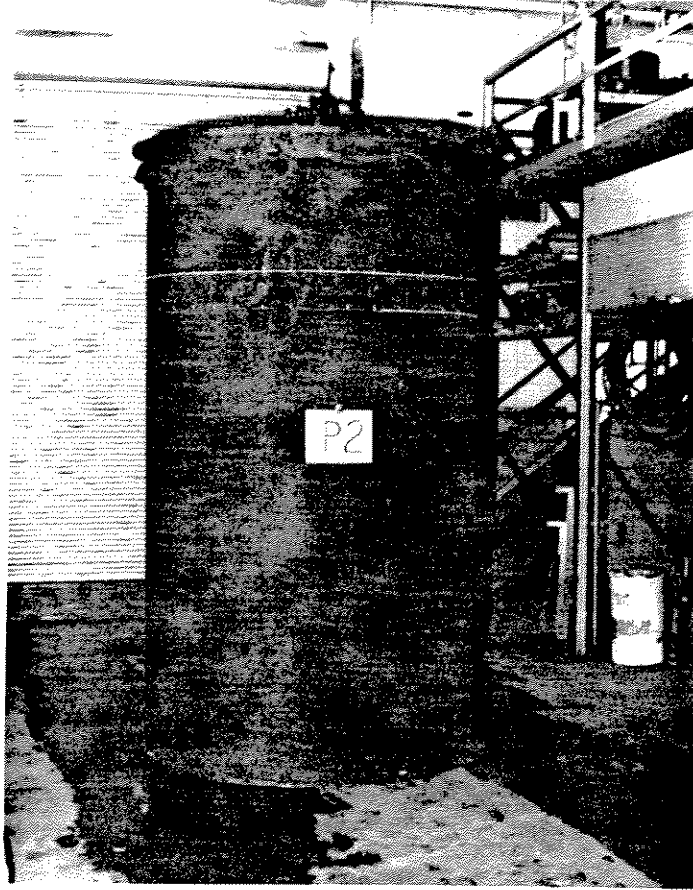


Figure 1: Specimen P2 Before Modification

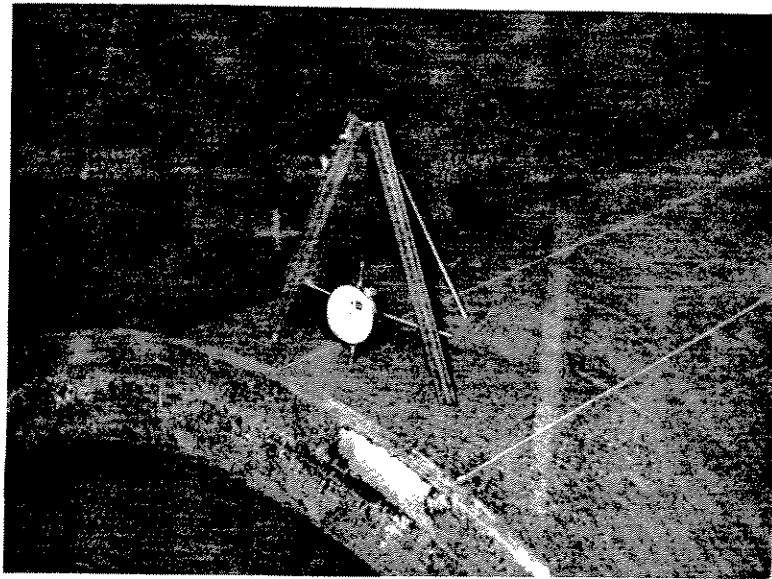


Figure 2: Device Used for Circumferential Measurements of Specimen P2

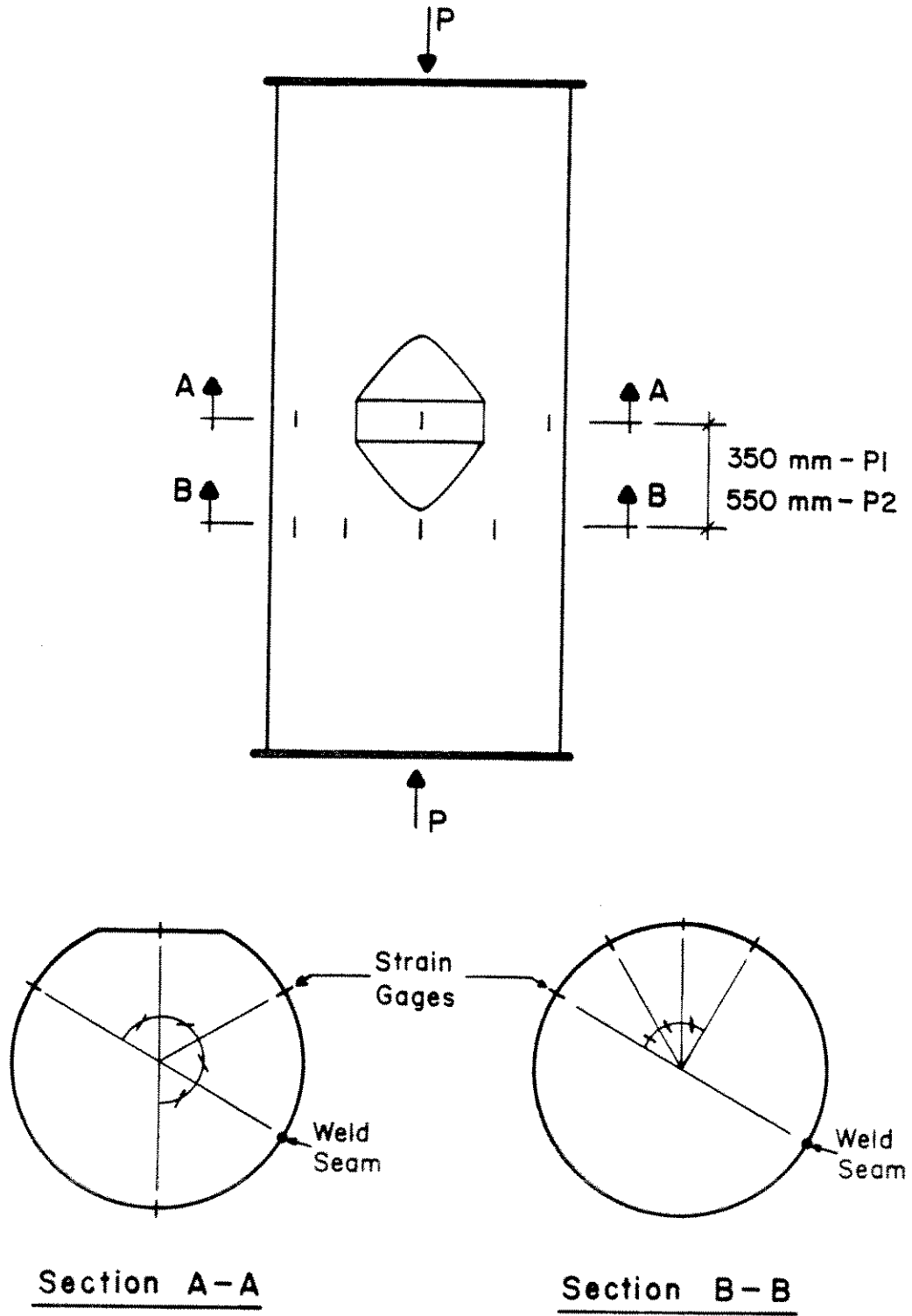


Figure 3: Location of Strain Gages

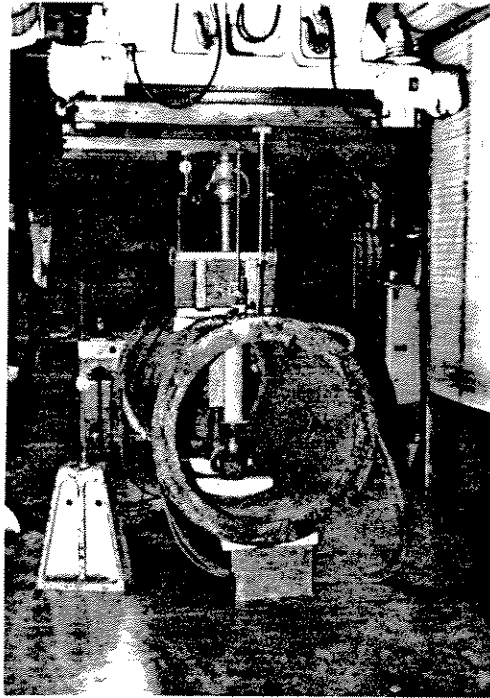


Figure 4: Set-up for Indentation of Specimen P1

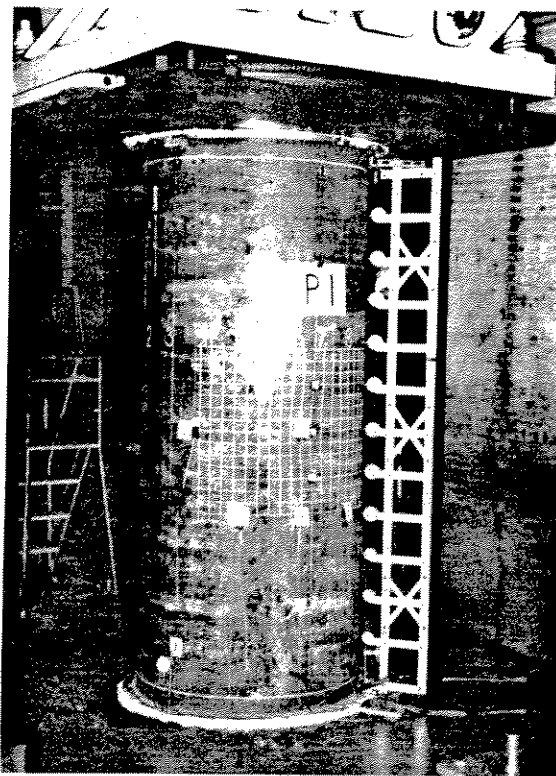


Figure 5: Axial Load Test Set-up for Specimen P1

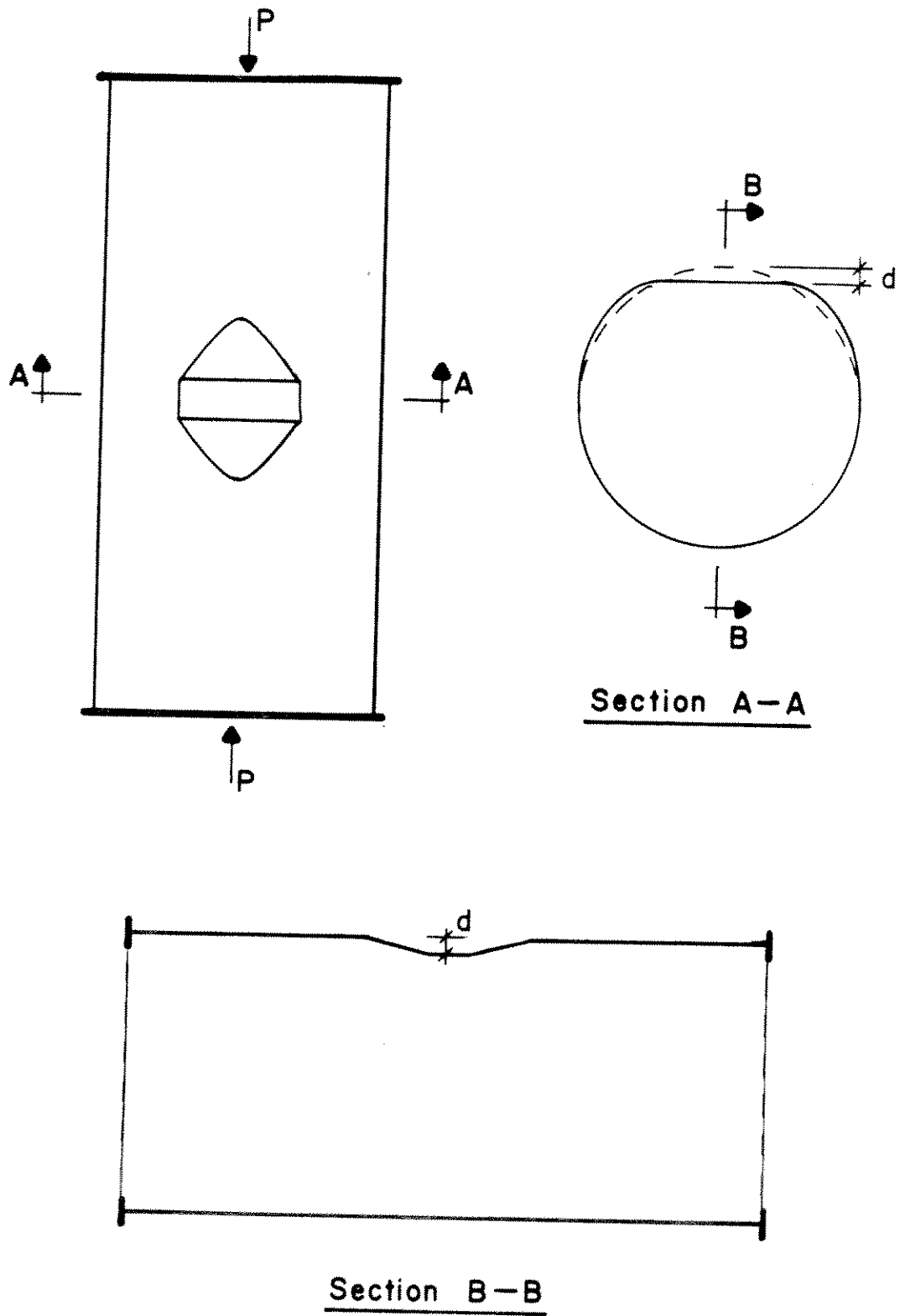


Figure 6: Schematic Representation of Ideal Dent Geometry



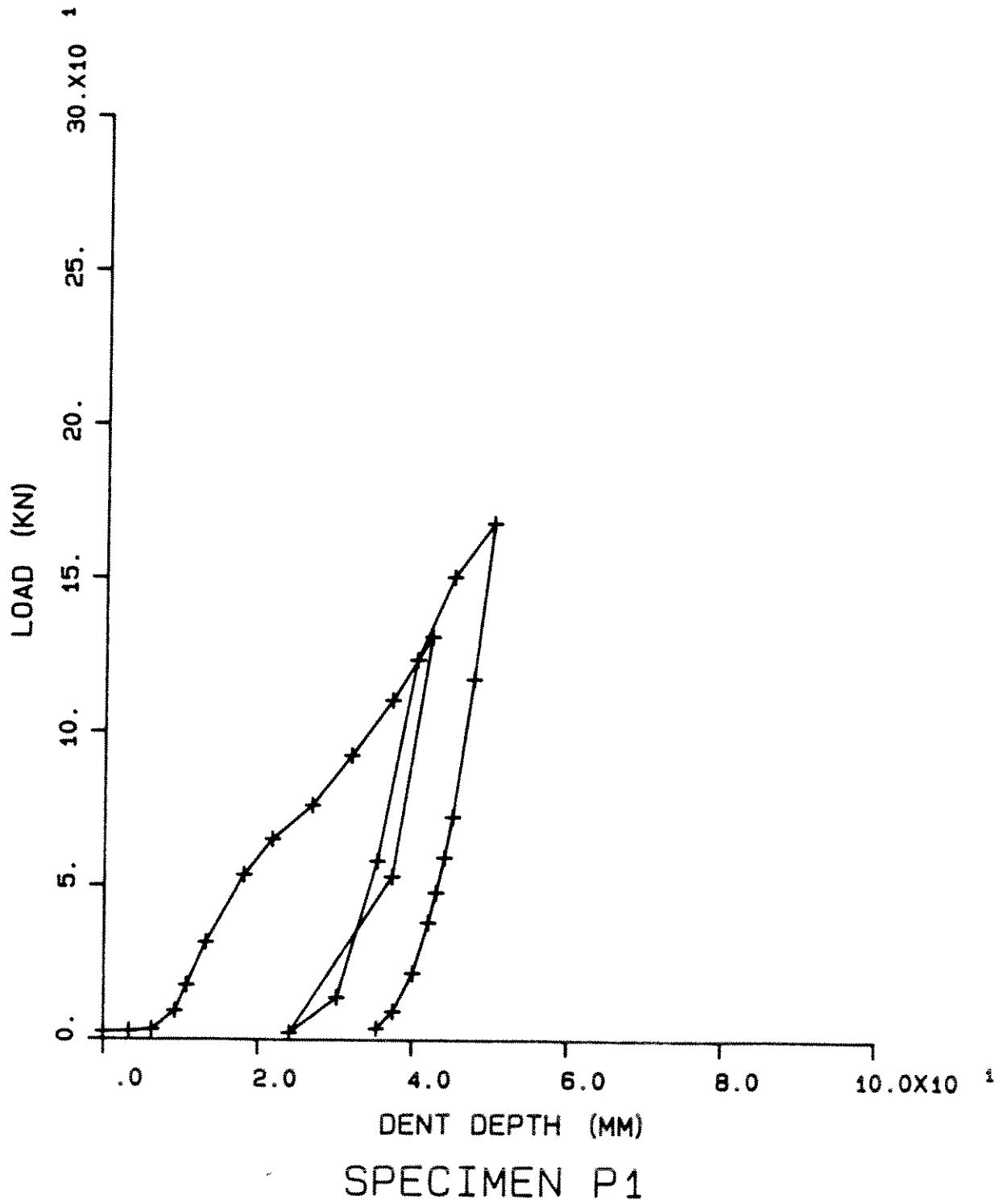


Figure 8: Load-Displacement Curve for Indentation of Specimen P1

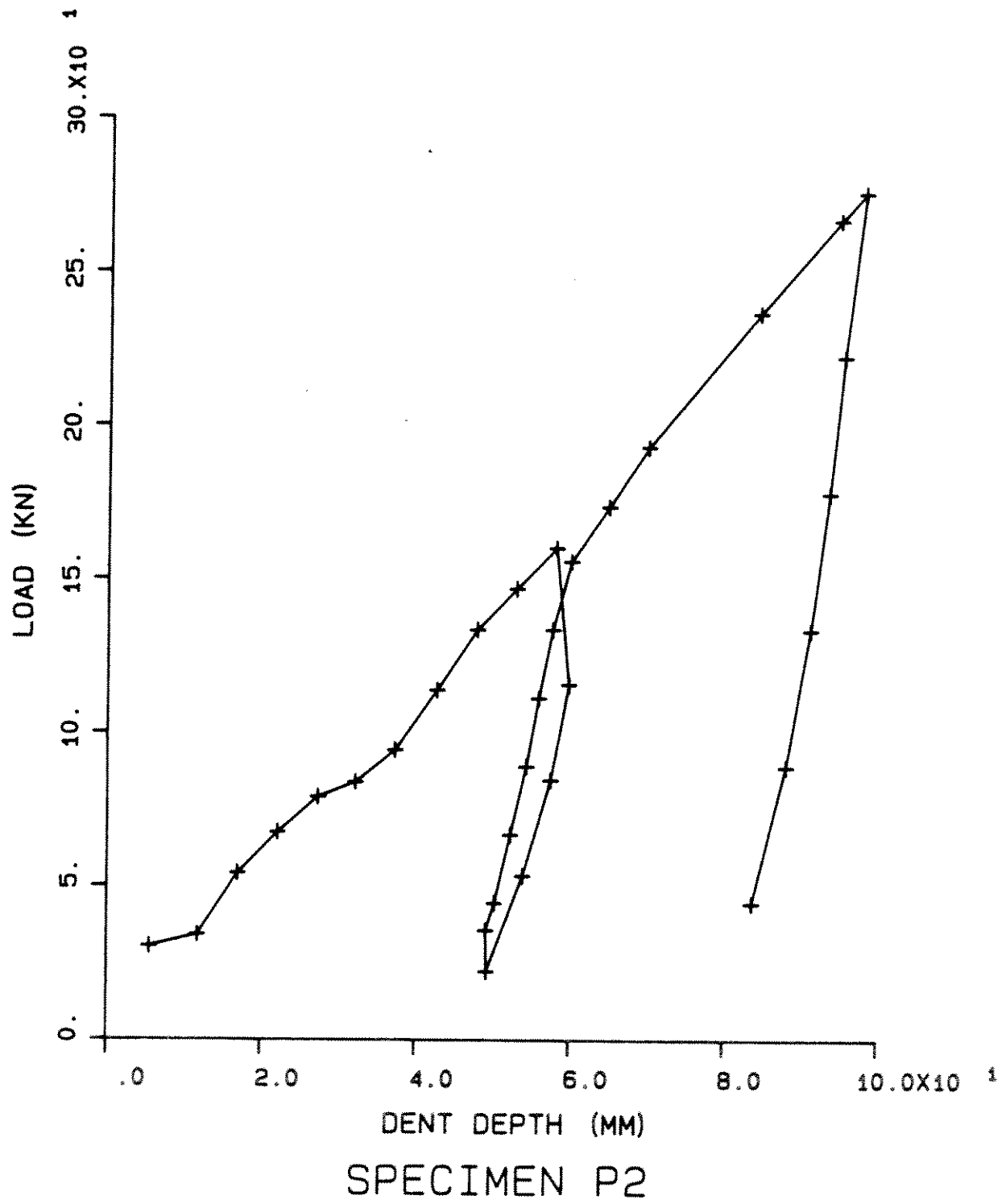
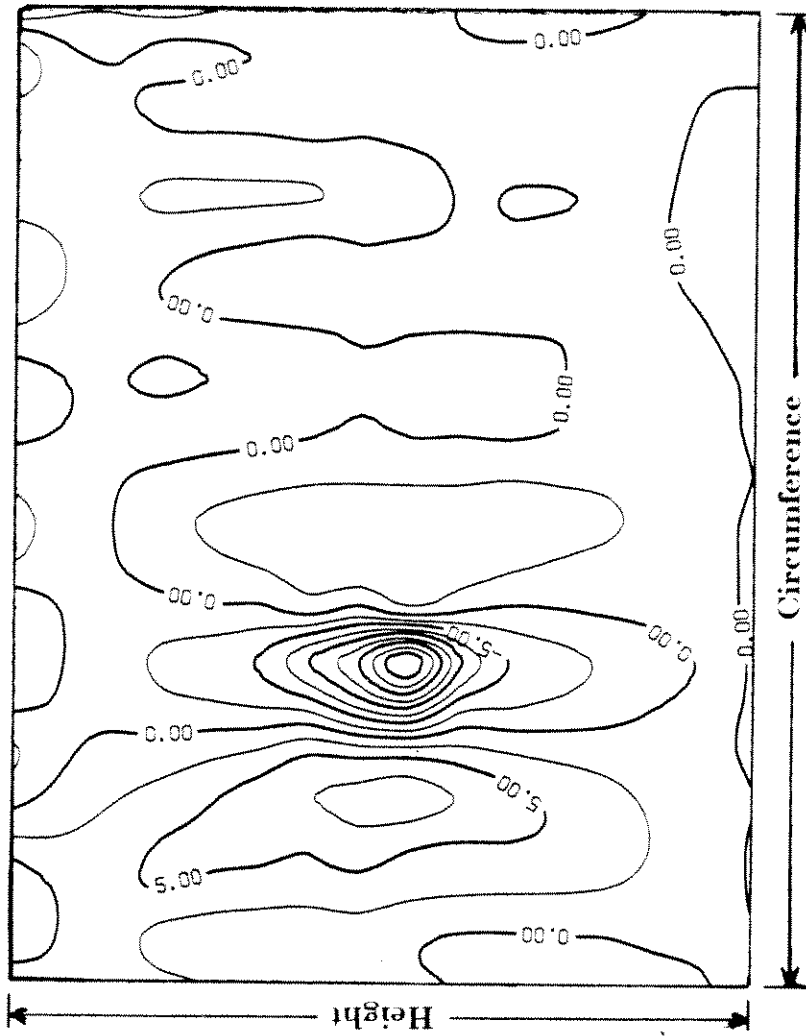
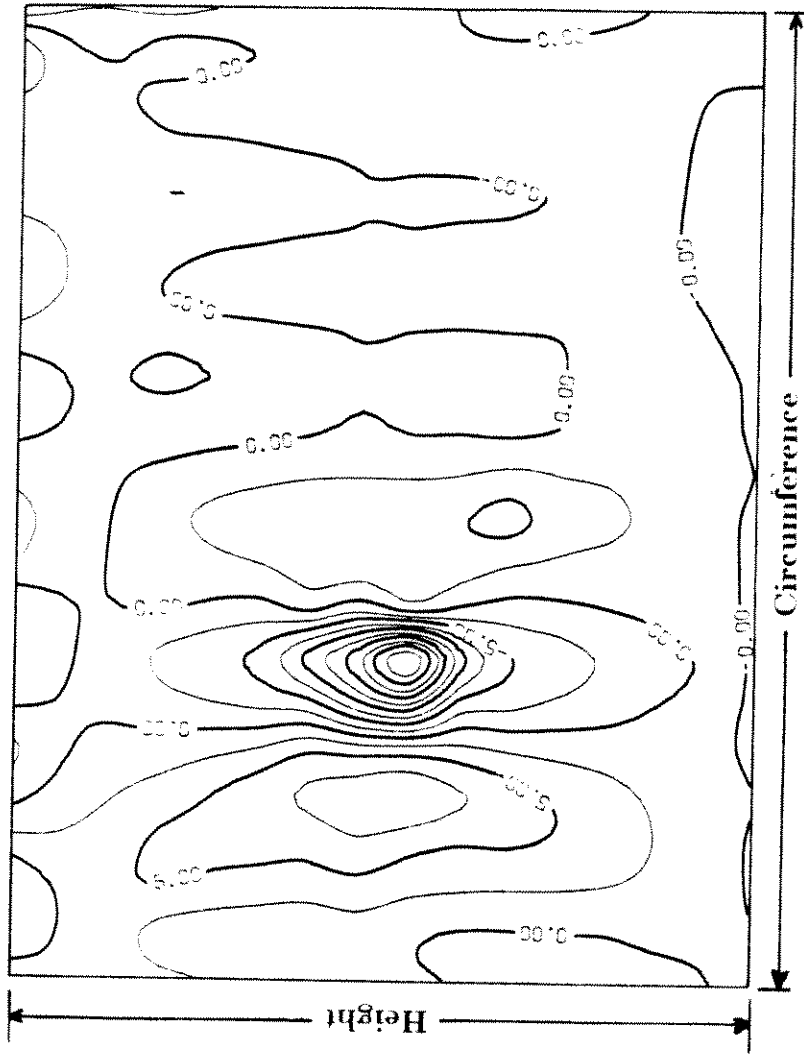


Figure 9: Load-Displacement Curve for Indentation of Specimen P2



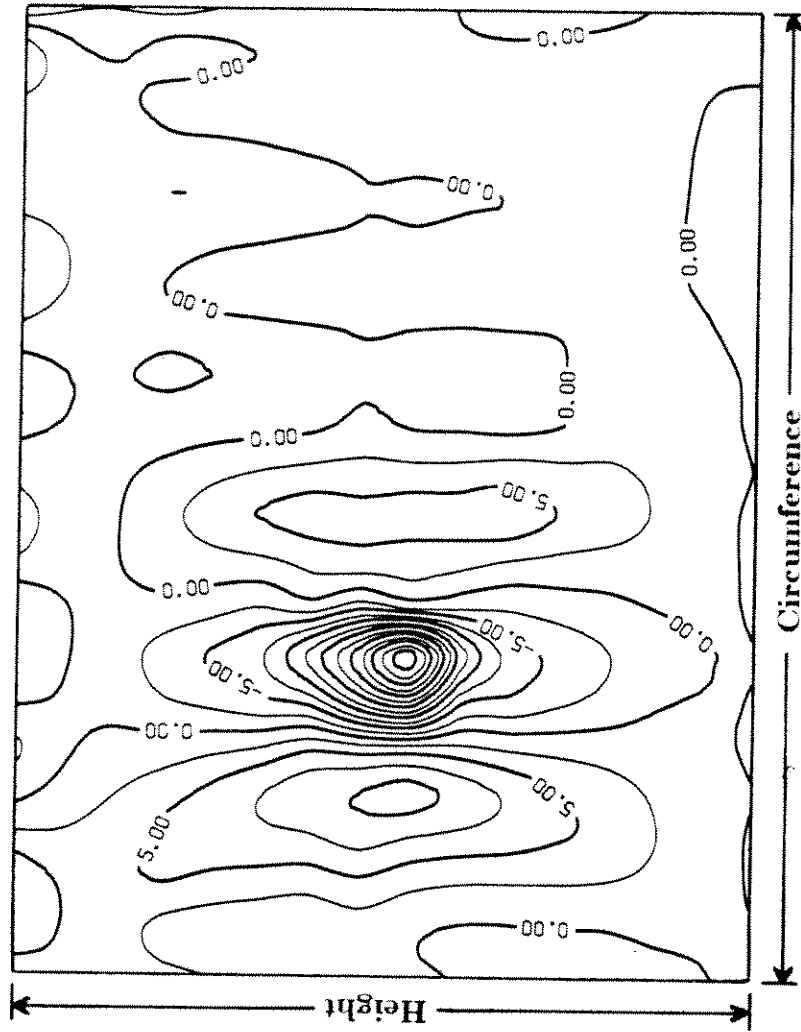
### Surface Contours (mm)

Figure 10: Contour Plot of Specimen P1 at 0 kN Axial Load



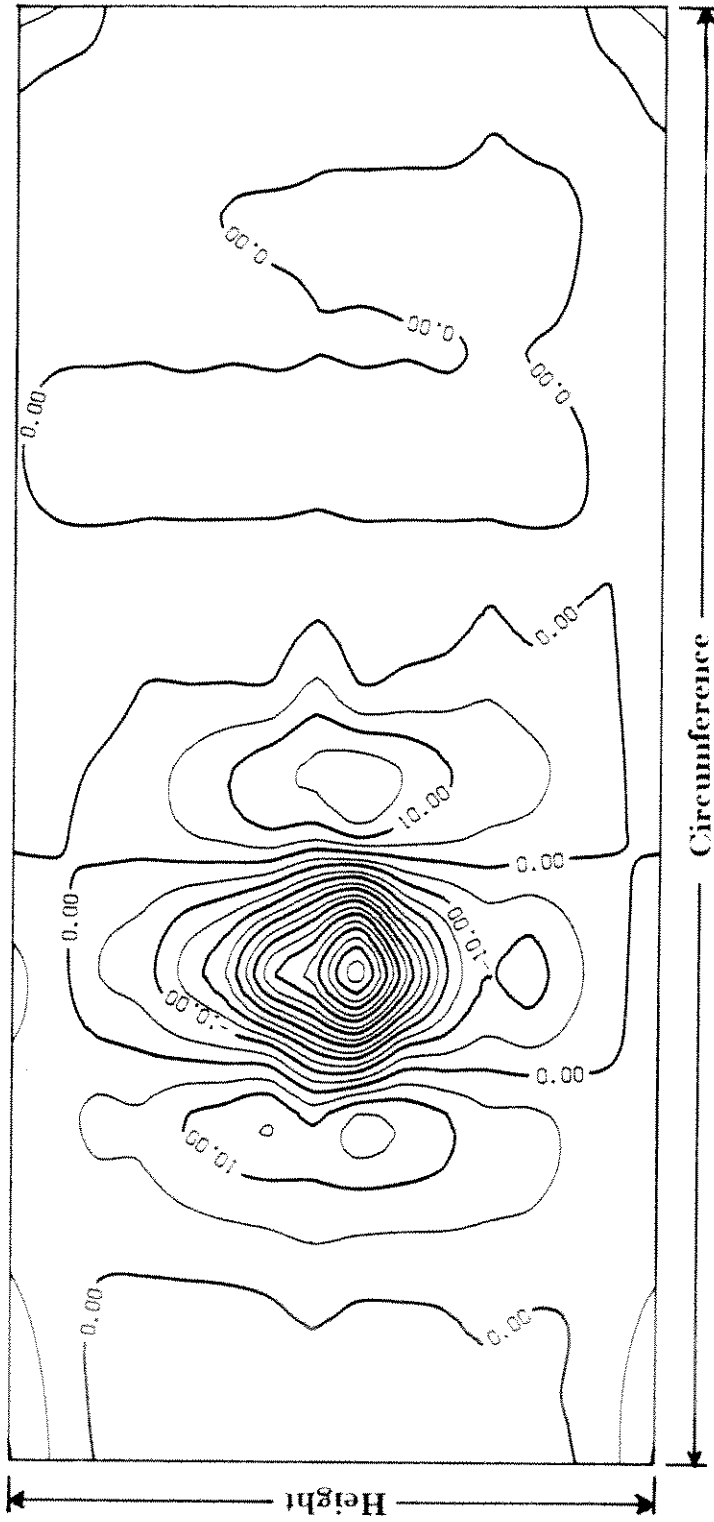
### Surface Contours (mm)

Figure 11: Contour Plot of Specimen P1 at 2230 kN Axial Load



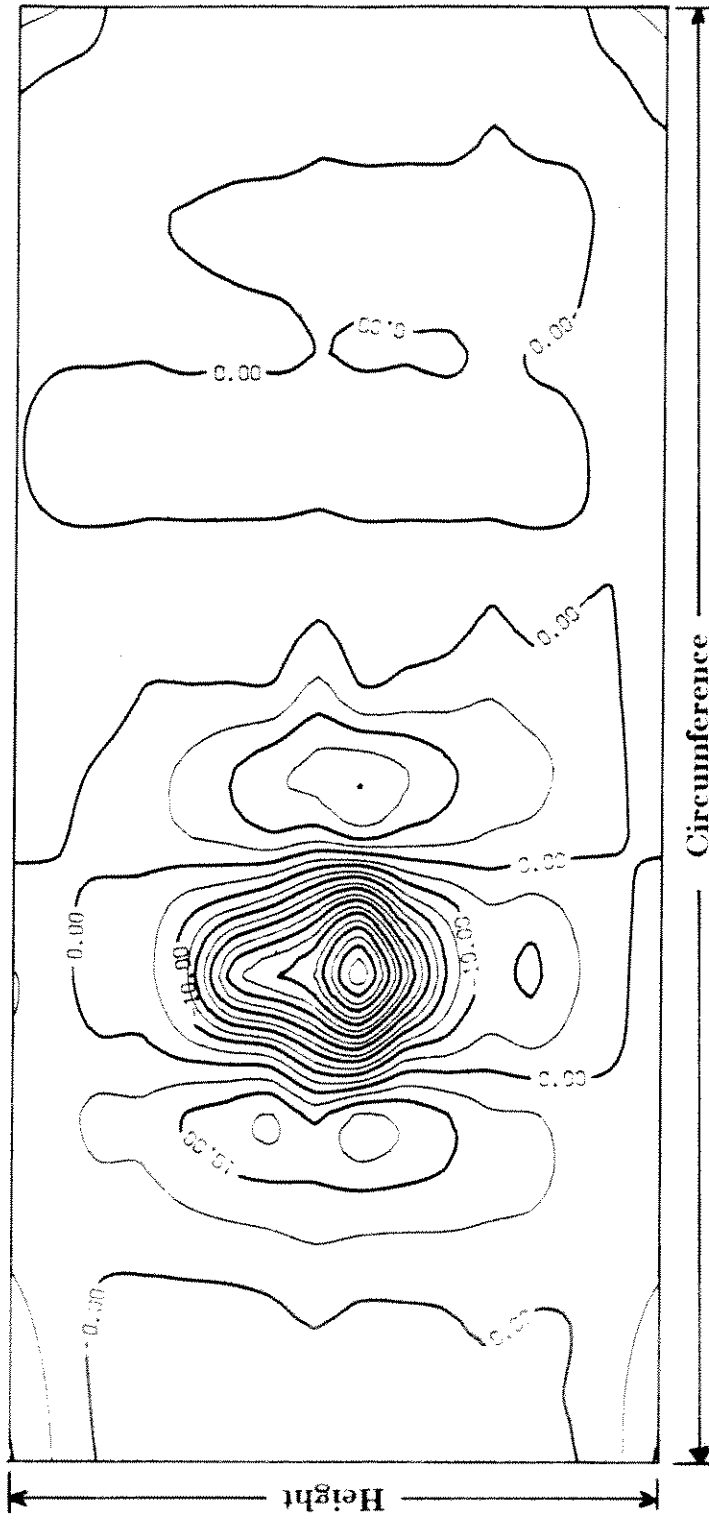
### Surface Contours (mm)

Figure 12: Contour Plot of Specimen P1 at 4450 kN Axial Load



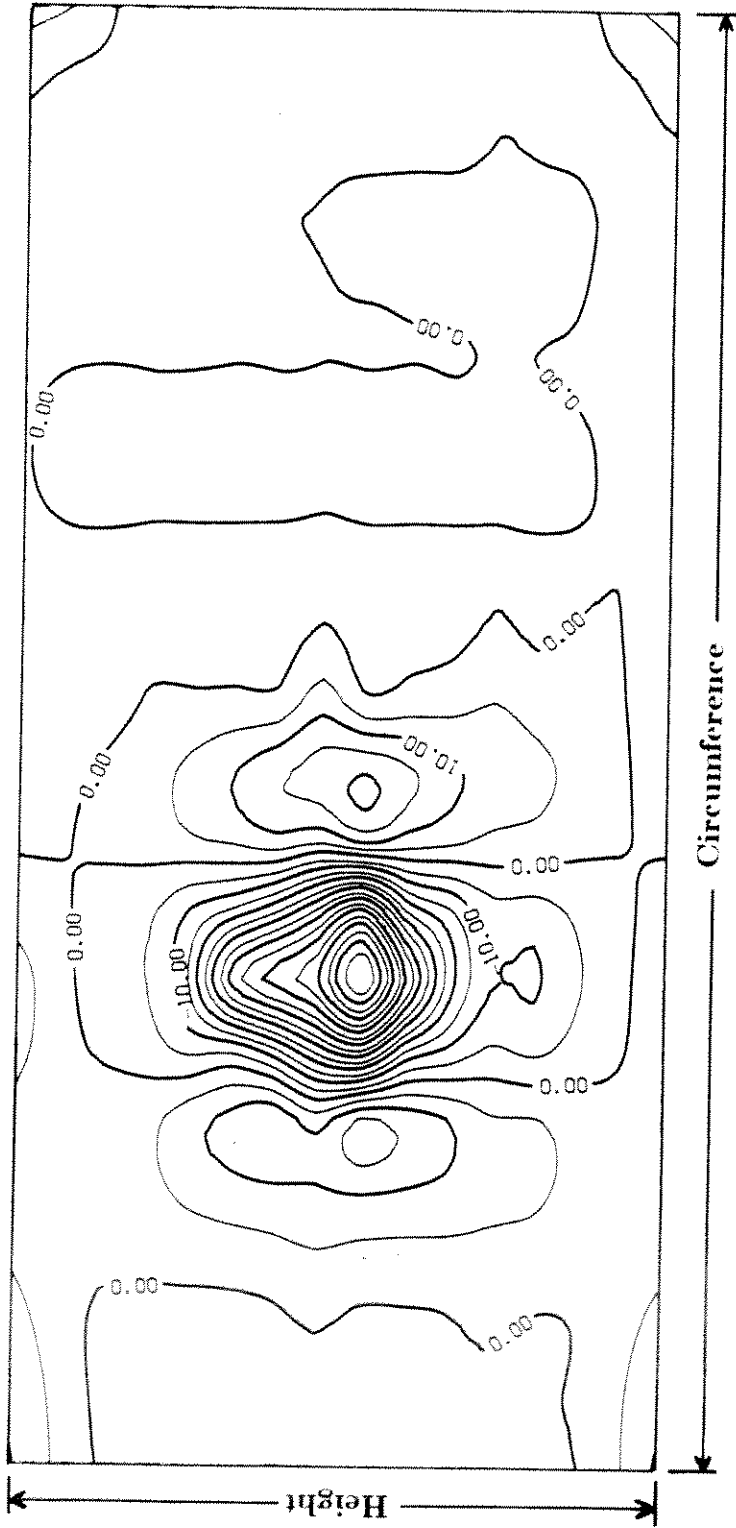
### Surface Contours (mm)

Figure 13: Contour Plot of Specimen P2 at 0 kN Axial Load



Surface Contours (mm)

Figure 14: Contour Plot of Specimen P2 at 2230 kN Axial Load



### Surface Contours (mm)

Figure 15: Contour Plot of Specimen P2 at 4450 kN Axial Load

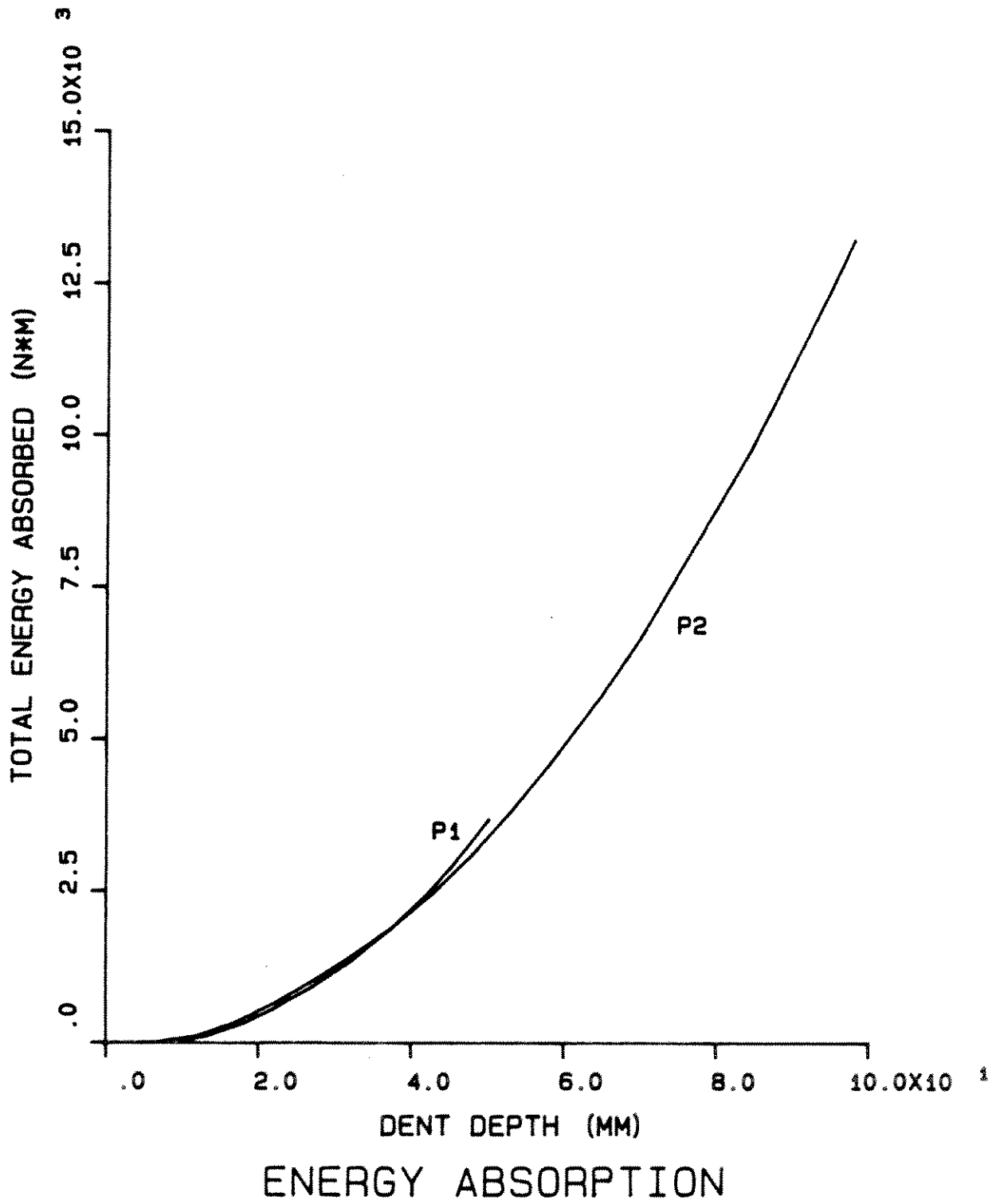


Figure 16: Energy Absorption vs. Dent Depth for Specimens P1 and P2

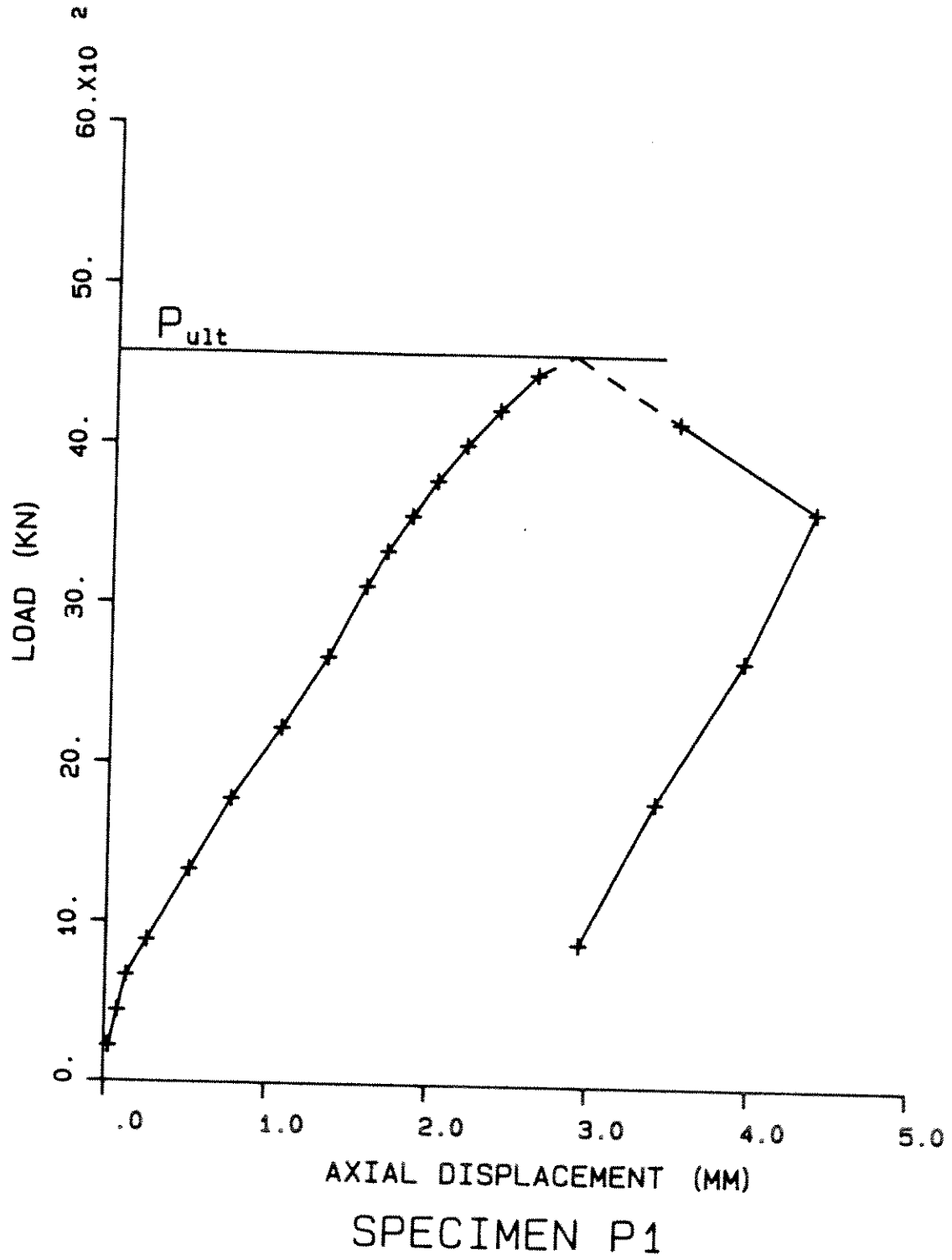


Figure 17: Load vs. Axial Shortening Curve for Specimen P1

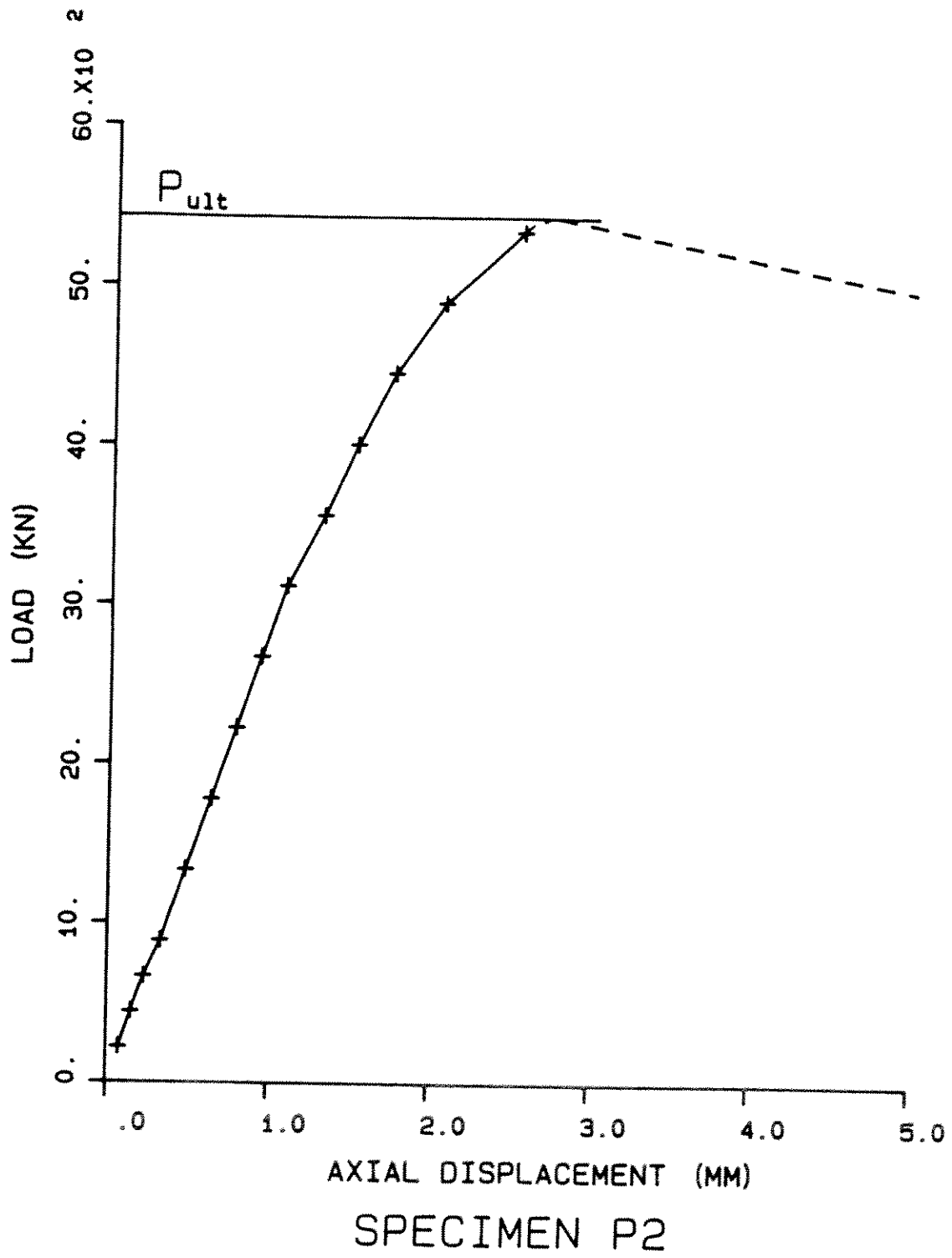
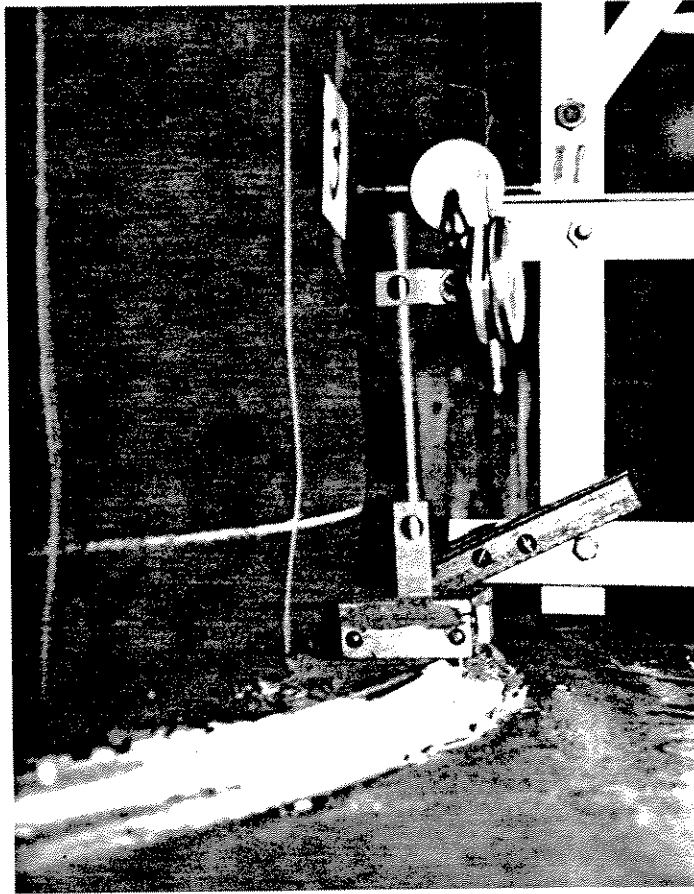


Figure 18: Load vs. Axial Shortening Curve for Specimen P2



**Figure 19:** Formation of Ring Bulge on Specimen P1

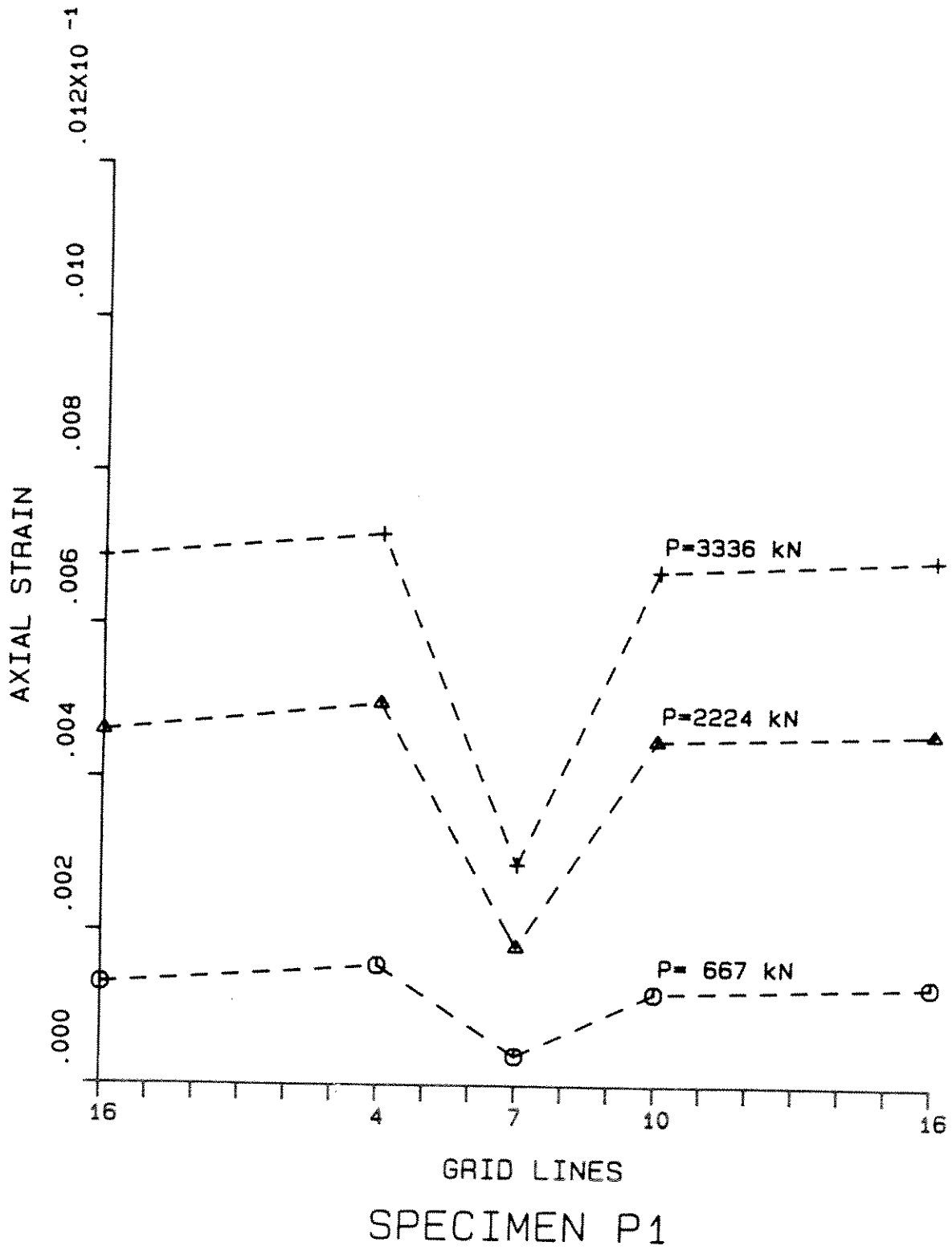


Figure 20: Axial Strains, Specimen P1

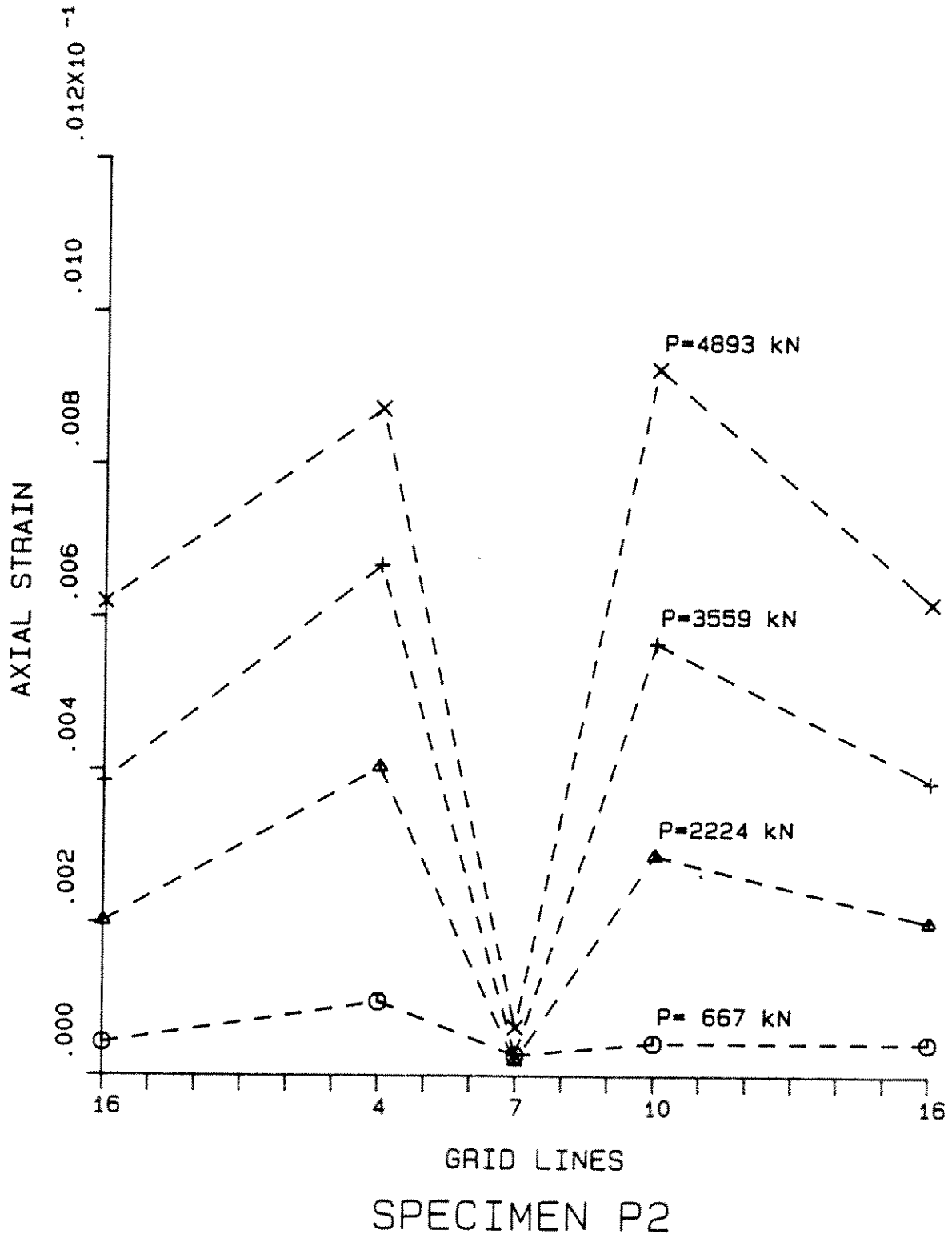


Figure 21: Axial Strains, Specimen P2